International Journal of Heat and Mass Transfer 244 (2025) 126981

Contents lists available at ScienceDirect

International Journal of Heat and Mass Transfer

journal homepage: www.elsevier.com/locate/ijhmt

Numerical study on pseudo-boiling heat transfer of supercritical CO_2 in horizontal tube

Bowen Yu [a], Jian Xie [a,*], Jinliang Xu [a,b], Liangyuan Cheng [a]

[a] Beijing Key Laboratory of Multiphase Flow and Heat Transfer for Low Grade Energy Utilization, North China Electric Power University, Beijing 102206, China
[b] Key Laboratory of Power Station Energy Transfer Conversion and System of Ministry of Education, North China Electric Power University, Beijing 102206, China

ARTICLE INFO

Keywords:
Supercritical CO_2
Pseudo-boiling
Heat transfer deterioration
Phase distribution
Non-uniform temperature distribution

ABSTRACT

Supercritical carbon dioxide sCO_2 is an attractive fluid candidate for power generation systems to achieve higher efficiency. The heat transfer performance of sCO_2 is of significant concern. Here, sCO_2 with pressure ranging from 8−12 MPa heated in 10.0 mm diameter horizontal tube is investigated numerically. The mass flux and heat flux ranges are 300−700 kg/m^{2}s, 70−210 kW/m^2, respectively. Based on the pseudo-boiling concept, phase distribution of supercritical fluid is obtained, which involves a liquid-like (LL) core and a vapor-like (VL) layer on the tube wall. The thickness of VL layer is the key to the heat transfer of supercritical fluid, which is determined by the balance of evaporation momentum force and inertia force. For high heat flux, large evaporation momentum force induces thick and wavy VL layer, resulting in heat transfer deterioration HTD. Along the flow direction, there is wall temperature overshoot with the maximum value of 114.2 ^{o}C. What's worse, the thickness of VL layer in the horizontal tube is non-uniform in the circumferential direction. The VL layer at the top of tube is thicker and the wall temperature is much higher. The circumferential wall temperature difference reaches 138.7 ^{o}C, maximally. As potential safety hazards for heat transfer exchangers, both wall temperature overshoot and non-uniformity need to be suppressed. The results show that rising pressure only reduces wall temperature value but has a weak impact on non-uniformity. Increasing mass flux raises the inertia force to compete against the evaporation momentum force, yielding thin and smooth VL layer, decreasing both wall temperature overshoot and non-uniformity. In brief, this work not only reveals HTD mechanism of supercritical fluid based on pseudo-boiling theory, but also guides the safety design of horizontal heat exchangers such as parabolic trough solar receivers using sCO_2.

1. Introduction

To combat global warming, traditional fossil fuel power plants need to improve the system efficiency, and clean energy such as solar thermal power should be exploited widely. Carbon dioxide is an attractive fluid candidate to replace water for power generation systems, due to its chemical inertness at high temperatures to achieve higher efficiency [1,2]. Carbon dioxide is also popular in the utilization of clean energy for the easier ability to reach a supercritical state [3,4]. However, several challenges are still on the way. The heat transfer performance of supercritical carbon dioxide sCO_2 is of significant concern. For example, the heat transfer deterioration (HTD) phenomenon occurs in horizontal tubes of parabolic trough solar receivers using sCO_2 as working fluid, inducing bend deformation and stress-rupture of tubes [5]. Thus, it is important to reveal the HTD mechanism for the safety operation of the sCO_2 power cycle.

It is noted that previous investigations have paid more attention to supercritical HTD in vertical tubes [6–10]. Different from normal heat transfer (NHT) under low heat flux, HTD under high heat flux behaves wall temperature peak along the flow direction [11]. In classical theory, supercritical fluid is treated as homogeneous single-phase flow. HTD is attributed to the buoyancy/acceleration effects caused by varied physical properties of supercritical fluid [12–15]. *Bu* number and *Ac* number are proposed for the buoyancy effect and acceleration effect, respectively [12,16]. However, Zhu et al [17]. point out that these non-dimensional numbers cannot judge the occurrence of HTD based on a quantity of experimental data from different references. The review papers investigating buoyancy criterion in recent years have also reached similar conclusions [18,19]. Thus, single-phase flow theory has limitations in clarifying the HTD mechanism of supercritical fluid.

In fact, supercritical fluid behaves inhomogeneous structure

* Corresponding author.
E-mail address: xiejian90@ncepu.edu.cn (J. Xie).

https://doi.org/10.1016/j.ijheatmasstransfer.2025.126981
Received 1 September 2024; Received in revised form 6 November 2024; Accepted 14 March 2025
Available online 20 March 2025

Nomenclature

c_p	specific heat capacity (J/kgK)
d	inner diameter of the tube (m)
d_{out}	outer diameter of the tube (m)
G	mass flux (kg/m^{2}s)
g	gravitational acceleration (m/s^2)
h	heat transfer coefficient (W/m^{2}K)
i	enthalpy (kJ/kg)
k	Turbulent energy (m^2/s^2)
K	non-dimensional number K,
m	mass flow rate (kg/s)
P	pressure (Pa)
ΔP	pressure drop (Pa)
Pr	Prandtl number
q_w	heat flux (W/m^2)
SBO	Supercritical boiling number
T	temperature (K)
T^-	the onset of pseudo-boiling temperature (K)
T^+	the termination of pseudo-boiling temperature (K)
t	time (s)
ΔT	wall temperature difference (K)
ΔV	volume change (m^3)
y	distance to the inner wall (m)
z	test tube length (m)

Greek symbol

δ	Vapor-like film thickness (m)
λ	thermal conductivity (W/m·K)
μ	kinematic viscosity (Pa·s)
θ	angle (°)
ρ	density (kg/m^3)

Subscript

b	bulk fluid
bot	bottom generatrix
exp	experimental data
fg	latent heat of evaporation
in	inlet
I′	inertia
l	liquid
M′	momentum
out	outlet
pc	pseudo-critical
pre	simulated value
top	top generatrix
v	vapor
wo	outer wall condition
wi	inner wall condition

Abbreviation

HTD	Heat transfer deterioration
LL	liquid-like
NHT	Normal heat transfer
sCO_2	supercritical carbon dioxide
TPL	two-phase-like
VL	vapor-like

according to more and more evidence from MD simulation [20,21], visualization experiments [22,23] and thermodynamic theory [24]. Wang et al [25]. proposed that the supercritical fluid is divided into three regimes including vapor-like (VL), liquid-like (LL) and two phase-like (TPL). Under continuous heating conditions, the structure of supercritical fluid changes from liquid-like to vapor-like, which is similar to the subcritical boiling phenomenon and named as pseudo-boiling [26,27]. Subcritical boiling occurs at one saturation temperature point. However, pseudo-boiling has a starting pseudo-boiling point temperature T^- and a ending pseudo-boiling point temperature T^+. For convective heat transfer of supercritical fluid in heating tube, when the fluid temperature near the tube wall reaches T^+, the vapor-like film with low thermal conductivity is generated. To characterize the vapor-like film thickness under the competition between evaporative momentum force and inertia forces, Zhu et al [28] proposed a new dimensionless number *SBO* and performed heating experiments of sCO_2 in vertical tube. It is surprising to find that there exists a critical *SBO* to identify NHT and HTD cases perfectly. What is more, such a method is satisfied for different supercritical fluids including CO_2, H_2O, R134a and R22 [29]. More recent investigations show that pseudo-boiling theory and multi-phase flow view are promising methods to reveal the supercritical HTD mechanism [30–37].

Different from HTD in vertical tube, HTD in horizontal tube induces not only wall temperature overshoot in flow direction, but also serious wall temperature non-uniformity in circumferential direction [38,39]. The problem becomes more complex. Adebiyi and Hall [40] performed heat transfer experiments of sCO_2 in horizontal tube. It is observed that the top wall temperatures are higher than the bottom wall temperatures. What is more, the circumferential wall temperature difference becomes remarkable when the pseudo-critical temperature is between the wall temperature and the fluid bulk temperature [41]. According to the classical theory, flow stratification and secondary flows induced by the buoyancy effect are used to explain the wall temperature non-uniformity for NHT case [42,43]. However, the reason for the sharp rise of wall temperature non-uniformity under HTD case is still unknown. Recently, Zhang et al [44] verified the similarity between subcritical boiling and supercritical pseudo-boiling of CO_2 in horizontal tubes. Cheng et al [45–47]. used the pseudo-boiling theory to explain the heat transfer difference between the top and the bottom of horizontal tube. It is found that experiment data of wall temperature non-uniformity in the circumferential direction is connected to *SBO*.

In summary, pseudo-boiling theory is promising to replace single-phase flow theory to clarify the supercritical HTD mechanism. However, the recent investigations focus on pseudo-boiling in vertical tubes. Here, heat transfer of sCO_2 in the horizontal tube is investigated numerically. Phase distribution of supercritical fluid is obtained to explain the supercritical HTD phenomenon, including the wall temperature overshoot in flow direction and serious wall temperature non-uniformity in circumferential direction. The effects of mass flux and pressure on pseudo-boiling of sCO_2 are also discussed. This work is meaningful to guide the safety design of horizontal heat exchanger such as parabolic trough solar receiver using sCO_2.

2. Mathematical model and calculation method

2.1. Physical model and grid generation

Fig. 1 shows the physical model of sCO_2 flow in the horizontal tube under uniform heating. The tube geometrical parameters remain the same as those of the experiment section in our previous investigation [45]. The horizontal tube is divided into three parts, including the inlet adiabatic section, heating section and outlet adiabatic section (see Fig. 1a). The length of the heating section is 3200 mm. The length of the inlet adiabatic section is 600 mm to ensure full development of sCO_2 before the heating section. The length of the outlet adiabatic section is also 600 mm to ensure the flow steady of sCO_2 at the outlet of the heating section. The flow direction is defined as z coordinate. The coordinate origin z=0 is at the inlet of the heating section. The tube's inner diameter and outer diameter are d=10 mm and d_{out}=14 mm, respectively (see Fig. 1b). The circumferential direction of the tube is defined as θ coordinate. $\theta = 0^\circ$ and $\theta = 180^\circ$ mean the top generatrix and bottom generatrix of the horizontal tube, respectively.

The three-dimensional model of the horizontal tube is meshed by ANSYS ICEM, using a structured hexahedral grid. The axial grids are uniform with the length of 20 mm. In order to increase the mesh quality and improve the calculation accuracy, the cross-section is divided by "O-shaped" grids (see Fig. 1c). The computing domain consists of two parts: fluid domain and solid domain. In order to obtain a better simulation effect, the mesh at the fluid-solid interface is refined. The thickness of the first layer of mesh is 10^{-7} m, and the growth ratio is 1.1 to ensure the dimensionless height of the first layer of mesh y^+<1 [48,49].

2.2. The governing equations

The three-dimensional steady flow and heat transfer of sCO_2 in the horizontal tube is simulated by ANSYS Fluent 19.2 software. The governing equations solved by finite volume method are as follows [50]:

Mass conservation equation

$$\frac{\partial}{\partial x_i}(\rho u_i) = 0 \tag{1}$$

Momentum conservation equation

$$\frac{\partial(\rho u_i u_j)}{\partial x_j} = -\frac{\partial P}{\partial x_i} + \frac{\partial}{\partial x_j}\left[(\mu + \mu_t)\left(\frac{\partial u_i}{\partial x_j} + \frac{\partial u_j}{\partial x_i} - \frac{2}{3}\delta_{ij}\frac{\partial u_k}{\partial x_k}\right)\right] + \rho g_i \tag{2}$$

Energy conservation equation

$$\frac{\partial(\rho u_i c_p T)}{\partial x_i} = \frac{\partial}{\partial x_i}\left[c_p\left(\frac{\mu}{Pr} + \frac{\mu_t}{Pr_t}\right)\frac{\partial T}{\partial x_i}\right] \tag{3}$$

where P and T are the pressure and temperature of fluid bulk, respectively. The physical properties of ρ, μ, c_p, Pr are the density, viscosity, specific heat, Prandtl number according to P and T. The parameters of μ_t and Pr_t are the turbulent viscosity and the turbulent Prandtl number. The parameter u is flow velocity and g is gravitational acceleration, respectively.

The numerical simulation accuracy of supercritical flow and heat transfer depends strongly on the turbulence model. According to the previous investigations [37,51–53], the shear stress transport SST k-ω model produces a more accurate prediction than other turbulence models. The SST k-ω transport equations are described as follows [54].

Turbulent kinetic energy equation

$$\frac{\partial(\rho \mu_i k)}{\partial x_i} = \frac{\partial}{\partial x_j}\left[\Gamma_k \frac{\partial k}{\partial x_j}\right] + G_k - Y_k \tag{4}$$

Specific dissipation rate equation

$$\frac{\partial(\rho u_i \omega)}{\partial x_i} = \frac{\partial}{\partial x_j}\left[\Gamma_\omega \frac{\partial \omega}{\partial x_j}\right] + G_\omega - Y_\omega + D_\omega \tag{5}$$

Further details about the variables and constants in Eqs. (4) and (5) can refer to the comprehensive discussion in Ref [54].

The all equations above only involve the fluid domain. For the solid domain, the Fourier's law of thermal conductivity equation is utilized, which is expressed as follows [55]

$$\frac{\partial}{\partial x_j}\left(\lambda_s \frac{\partial T}{\partial x_j}\right) + \Phi = 0 \tag{6}$$

where λ_s is the thermal conductivity of solid material. Φ represents the heat generation term, W/m^3.

2.3. Boundary conditions and solution

The physical properties of CO_2 are obtained from REFPROP NIST 9.1 [56]. The tube inlet is modeled using a mass flux condition, while the tube outlet is set as an outflow boundary. For the heating section of horizontal tube, a uniform heat flux applies on the solid outer wall. At the fluid-solid interface, the temperature and heat flux are continuous with no-slip condition:

$$T_f = T_s \tag{7}$$

$$\lambda_s \frac{\partial T}{\partial n} = \lambda_f \frac{\partial T}{\partial n} \tag{8}$$

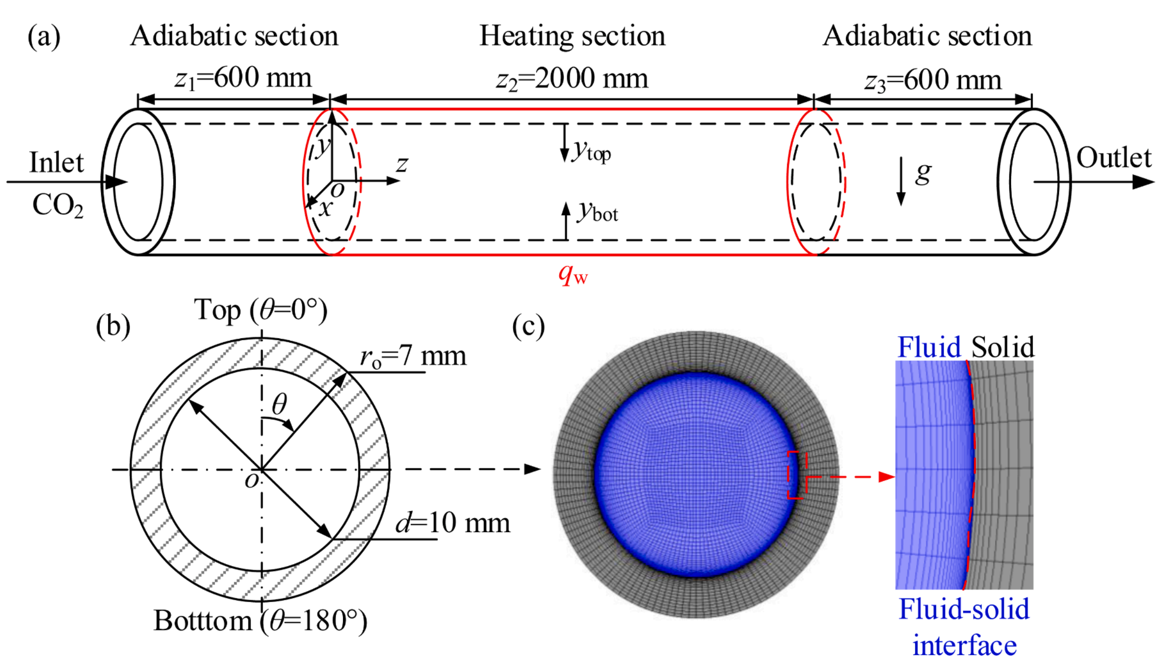

Fig. 1. Physical model and computational grid adopted in the numerical simulation: (a) Physical model; (b) Schematic of the inlet section; (c) Mesh configuration of cross section.

where subscripts of f and s represent fluid and solid, respectively.

The governing equations are discretized using the finite volume method. To enhance the accuracy of the calculations, a second-order upwind differencing scheme is employed. The pressure-velocity coupling is solved using the SIMPLEC algorithm. Convergence is identified when the residual curves stabilize and the monitored outlet temperature curve approaches a steady state. The relative residuals for the mass and momentum transport equations are set to 10^{-3}, while the relative residual for the energy transport equation is set to 10^{-9}.

2.4. Parameter definition

The main parameters employed in the present work are defined as follows. The heating power Q is calculated by

$$Q = m(i_{\mathrm{out}} - i_{\mathrm{in}}) \tag{9}$$

where i_{in} and i_{out} represents the inlet and outlet local fluid enthalpy, m is the mass flow rate.

The heat flux on the inner wall of the horizontal tube is as follows:

$$q_{\mathrm{w,ave}} = \frac{Q}{\pi d_{\mathrm{in}} z_2} \tag{10}$$

The calculation of the local heat transfer coefficient in a horizontal tube is defined as

$$h = \frac{q_{\mathrm{w,ave}}}{T_{\mathrm{wi}} - T_{\mathrm{b}}} \tag{11}$$

The calculation of the temperature of fluid bulk is performed as follows:

$$T_{\mathrm{b}} = \frac{\int_A \rho u c_{\mathrm{p}} T \mathrm{d}A}{\int_A \rho u c_{\mathrm{p}} \mathrm{d}A} \tag{12}$$

The enthalpy value of fluid bulk is

$$i_{\mathrm{b}} = \frac{\int_A \rho u i \mathrm{d}A}{\int_A \rho u \mathrm{d}A} \tag{13}$$

2.5. Validation of grid independence

To ensure the validity and accuracy of the simulated results, grid independence analysis is performed. The heat transfer coefficient at the top of the tube (h_{top}) and the heat transfer coefficient at the bottom of the tube (h_{bot}) under five different grid systems are calculated. Table 1 shows the results of grid independence analysis for both G=300 kg/m^2/s and G=700 kg/m^2/s, which are minimum and maximum flow rate in our simulation investigation, respectively. Considering the balance between computational efficiency and result accuracy, the final decision was made to utilize 2.55×10^6 grids for the simulation calculations.

2.6. Model validation

The experimental data from Ref [45,46]. are selected to validate the numerical simulation. The all geometric parameters of heating horizontal tubes are the same between the experiment and simulation. Fig. 2 shows the model validation result of outer wall temperature along the top and bottom generatrixes of the horizontal tube under various operating conditions. Fig. 2a and Fig. 2b are NHT cases and Fig. 2c is the HTD case. For both NHT and HTD cases, the simulated curves behave a similar trend to the dots of experimental data along the flow direction. For quantitative analysis, the mean relative error e_{A} between the simulated values and experimental data is defined as

$$e_A = \frac{1}{n}\sum_{i=1}^{n} e_i \times 100\% \tag{14}$$

The error at a location of z is e_i=$(T_{\mathrm{wo,\ pre}}-T_{\mathrm{wo,\ exp}})/T_{\mathrm{wo,\ exp}}$, where $T_{\mathrm{wo,\ pre}}$ and $T_{\mathrm{wo,\ exp}}$ are simulated value and experimental data of outer wall temperature, respectively. As a result, the maximum average deviation e_{A} is only 3.13%. The model validation of pressure drop ΔP under various operating conditions is also performed in Fig. 3. The mean relative error e_{A} between the simulated values and experimental data is also less than 3.82%. Thus, the numerical model employed in this study is reliable.

3. Results and discussion

3.1. Heat transfer performance of sCO_2 in horizontal tube

The heat transfer performance of sCO_2 in horizontal tubes is of significant concern for the safety design of heat exchangers such as parabolic trough solar receivers. Fig. 4 shows the variation of temperature and heat transfer coefficient along the flow direction under different heat flux at P=8 MPa, G=300 kg/m^{2}s. For low heat flux of q_{w}=70 kW/m^2, the wall temperatures rise gradually along the flow direction, performing normal heat transfer NHT (see Fig. 4a). However, for high heat flux of q_{w}=210 kW/m^2, the wall temperatures along the flow direction exhibit a noticeable peak, inducing heat transfer deterioration HTD. The maximum value of wall temperature overshoot reaches 114.2 °C (see point A in Fig. 4b). For both NHT and HTD cases in horizontal tube, the wall temperatures at the top generatrix $T_{\mathrm{wi,\ top}}$ are always higher than those at the bottom generatrix $T_{\mathrm{wi,\ bot}}$. The maximal temperature difference ΔT between $T_{\mathrm{wi,\ top}}$ and $T_{\mathrm{wi,\ bot}}$ is 34.1 °C for the NHT case. Seriously, the maximal ΔT reaches 138.7 °C for the HTD case. In summary, HTD in horizontal tubes induces not only wall temperature overshoot in the flow direction, but also serious wall temperature non-uniformity in the circumferential direction.

According to the wall temperatures T_{wi} and fluid bulk temperatures T_{b}, the local heat transfer coefficients at the top generatrix h_{top} and these at the bottom generatrix h_{bot} along the flow direction are calculated. Overall, h_{bot} is always larger than h_{top} (see Fig. 4c and Fig. 4d). For the NHT case under q_{w}=70 kW/m^2, the heat transfer coefficient at top generatrix h_{top} decreases continuously along the flow direction (see Fig. 4c). However, the heat transfer coefficient at top generatrix h_{top} increases first and then reduces along the flow direction. The maximum value of h is obtained near the location where the fluid bulk temperature T_{b} achieves pseudo-critical temperature T_{pc}. For the HTD case under q_{w}=210 kW/m^2, both h_{top} and h_{bot} decrease first and then rise along the

Table 1
Grid independence analysis (P=8 MPa, q_{w}=70 kW/m^2).

Grid number (10^6)	G=300 kg/m^2/s				G=700 kg/m^2/s			
	h_{t} (W/m^{2}K)	h_{b} (W/m^{2}K)	e_{t} (%)	e_{b} (%)	h_{t} (W/m^{2}K)	h_{b} (W/m^{2}K)	e_{t} (%)	e_{b} (%)
0.62	516.04	720.79	2.77	2.87	3097.07	5370.15	3.08	2.92
1.46	518.81	724.96	2.24	2.31	3135.69	5400.31	1.87	2.37
2.55	521.61	729.18	1.72	1.74	3174.31	5488.47	0.66	0.78
3.10	521.73	729.38	1.70	1.72	3179.66	5491.23	0.59	0.73
3.84	530.75	742.15	0	0	3195.47	5531.84	0	0

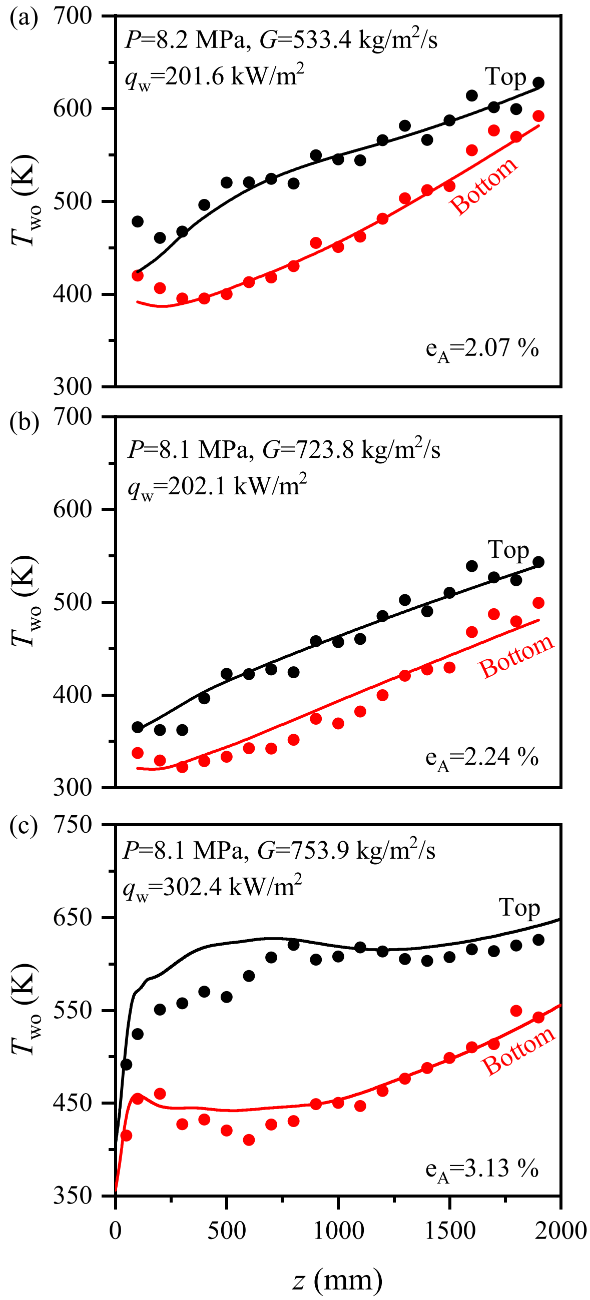

Fig. 2. Model validation result of the outer wall temperature T_{wo} along the flow direction z (the curves are simulated values and the dots are experimental data, experimental data in (a) are from Ref. [45], experimental data in (b) and (c) are from Ref. [46]).

flow direction (see Fig. 4d). What is more, the turning point is also near the location where T_b=T_{pc}.

3.2. Phase distribution of sCO_2 in cross-section

In brief, the variations of temperature and heat transfer coefficient are different at the top and bottom generatrix. They are also different under NHT and HTD cases. To explain the complex heat transfer performance of sCO_2 in the horizontal tube shown in Fig. 4, the promising

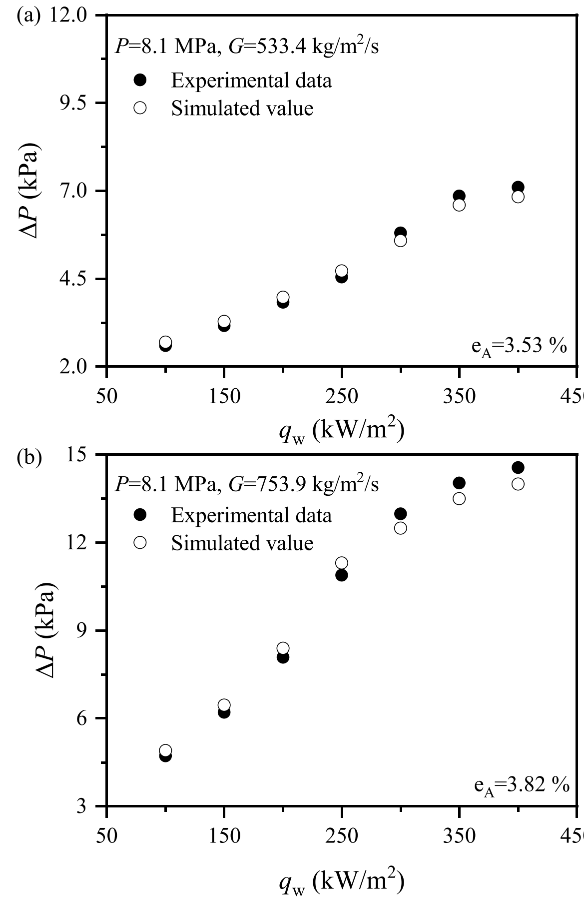

Fig. 3. Model validation result of pressure drop ΔP (the hollow dots are simulated values and the solid dots are experimental data from Ref. [46]).

method based on the pseudo-boiling concept is performed here. The most important issue is to identify the inhomogeneous structure distribution of supercritical fluid in horizontal tubes, including vapor-like (VL), liquid-like (LL) and two phase-like (TPL) [25]. Different from subcritical boiling, supercritical pseudo-boiling has two pseudo-boiling points under constant pressure, involving a starting temperature T^- and an ending temperature T^+. The supercritical fluid bulk behaves LL structure when its temperature is below T^-, and fluid bulk changes to VL structure when its temperature is larger than T^+.

Fig. 5 shows the thermodynamic method to determine the temperatures of T^- and T^+ [24]. Taking sCO_2 at P=8 MPa as an example (see Fig. 5a), the black curve presents the variation of specific enthalpy i versus temperature T based on NIST standard reference database (version 9.0) [56]. The two red straight lines are asymptotes of the black i-T curve. The top asymptote named $i_{G\text{-}asy}$-T line is for the ideal gas-phase and the bottom asymptote named $i_{L\text{-}asy}$-T line is for the ideal liquid-phase, respectively. The blue line is the tangent line of the black i-T curve. The tangency point is just pseudo-critical point with coordinate position of (T_{pc}, i_{pc}), which is marked as the black solid dot in Fig. 5a. The blue tangent line and the red asymptote of $i_{L\text{-}asy}$-T intersect at the point B to determine T^-. The blue tangent line and the red asymptote of $i_{G\text{-}asy}$-T intersect at point C to determine T^+. It is worth noting that there are T^- and T^+ for each supercritical pressure. Fig. 5b shows the black curve of P-T^- and the blue curve of P-T^+ to generate the phase diagram of sCO_2. Three regimes of LL, TPL and VL are identified in

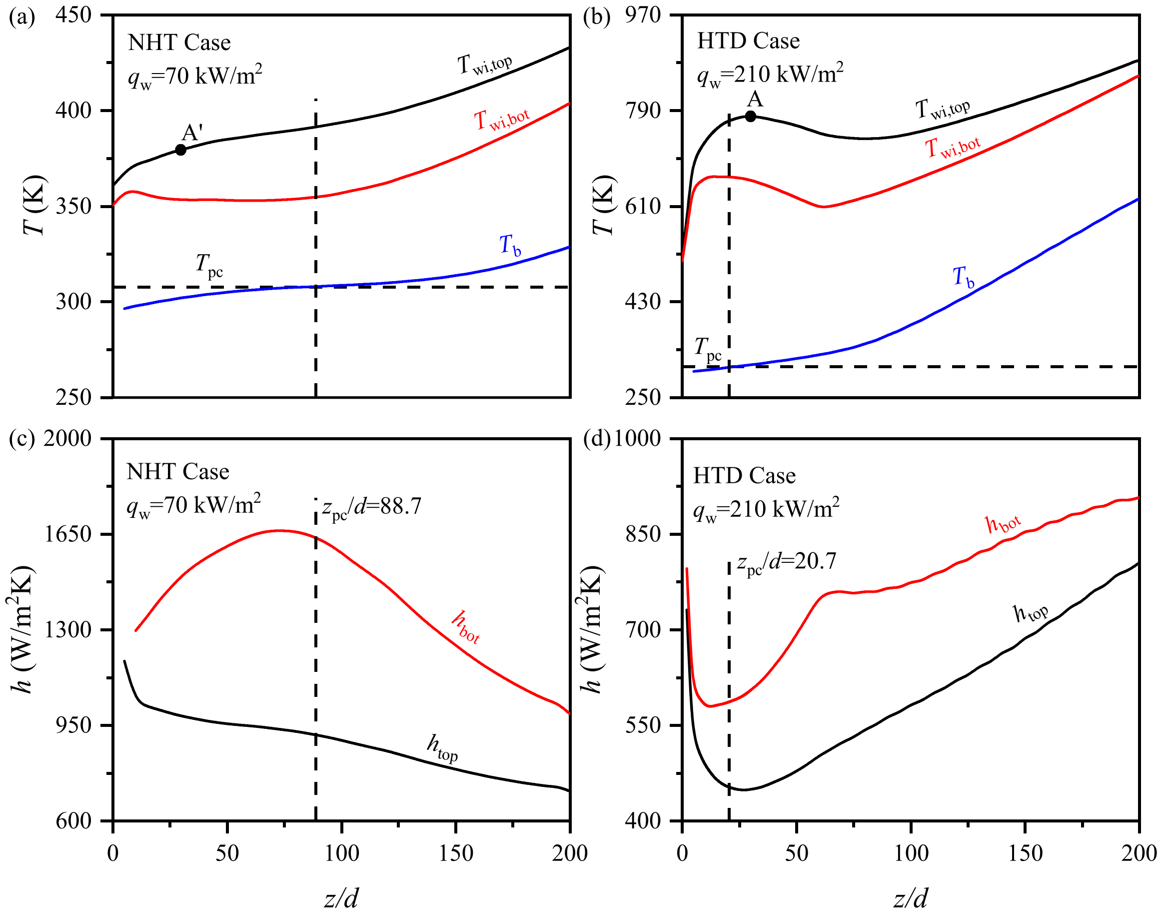

Fig. 4. Variation of the temperature and heat transfer coefficient along the flow direction under different heat flux (P=8 MPa, G=300 kg/m^{2}s): (a) and (c) are normal heat transfer NHT case under heat flux of 70 kw/m^2; (b) and (d) are heat transfer deterioration HTD case under heat flux of 210 kw/m^2.

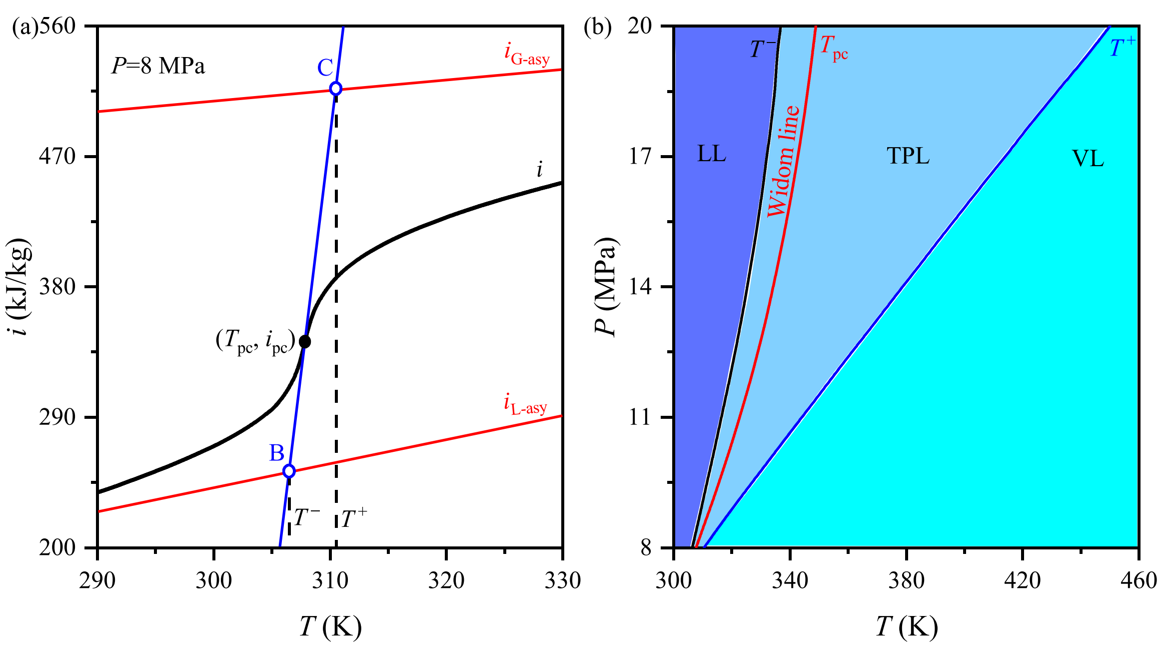

Fig. 5. Thermodynamic behavior of Supercritical CO_2: (a) Calculation method for pseudo-boiling temperatures T^- and T^+ based on Ref. [24]; (b) P-T phase diagram for CO_2.

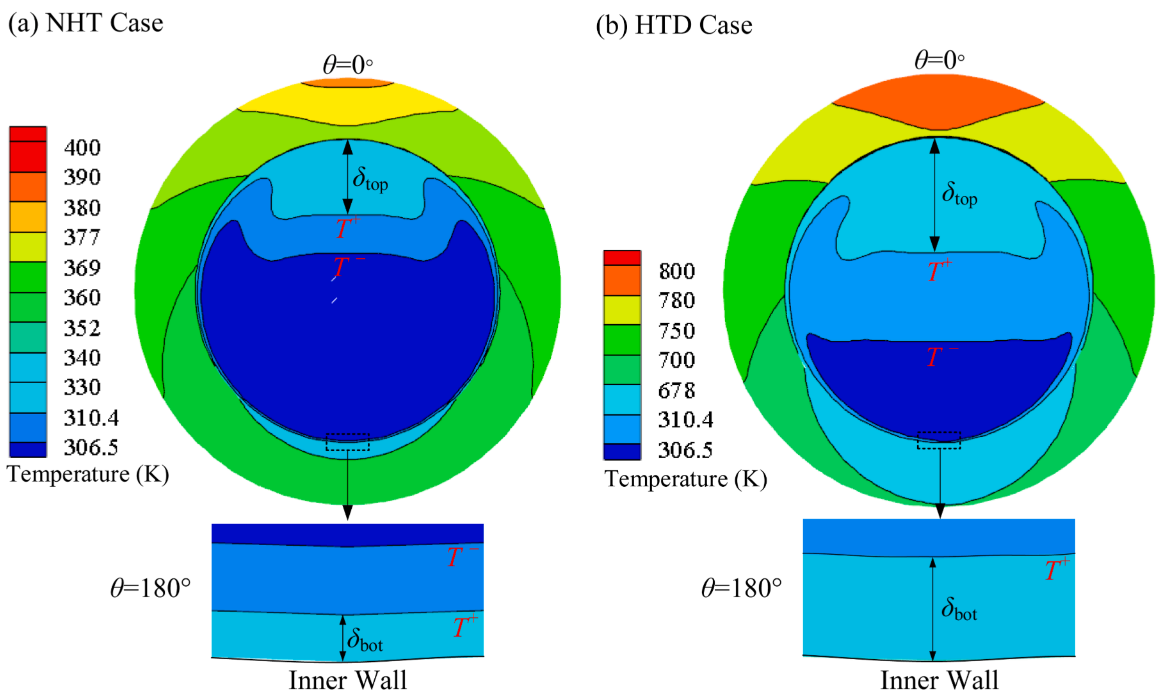

Fig. 6. Temperature fields and phase distributions at the cross section of z/d=30: (a) NHT case; (b) HTD case.

the phase diagram with $T<T-$, $T-<T<T^{+}$ and $T>T^{+}$, which are analogous to liquid, two-phase and vapor in subcritical pressure, respectively.

The phase diagram in Fig. 5b provides an important method to identify the inhomogeneous structures of supercritical fluid in horizontal tubes. The phase distribution is just based on pressure and temperature fields, which is easy to obtain by numerical simulation. Fig. 6 shows the temperature field of the tube wall and phase distribution of supercritical fluid bulk in the horizontal tube at the cross-section of z/d=30, where the wall temperature overshoot reaches a maximum value for HTD case at P=8 MPa, G=300 kg/m^{2}s, q_w=210 kW/m^2 (see point A in Fig. 4b). Heated by the tube, the fluid near the tube wall behaves with rising temperature to reach T^+ firstly, generating VL film with low heat

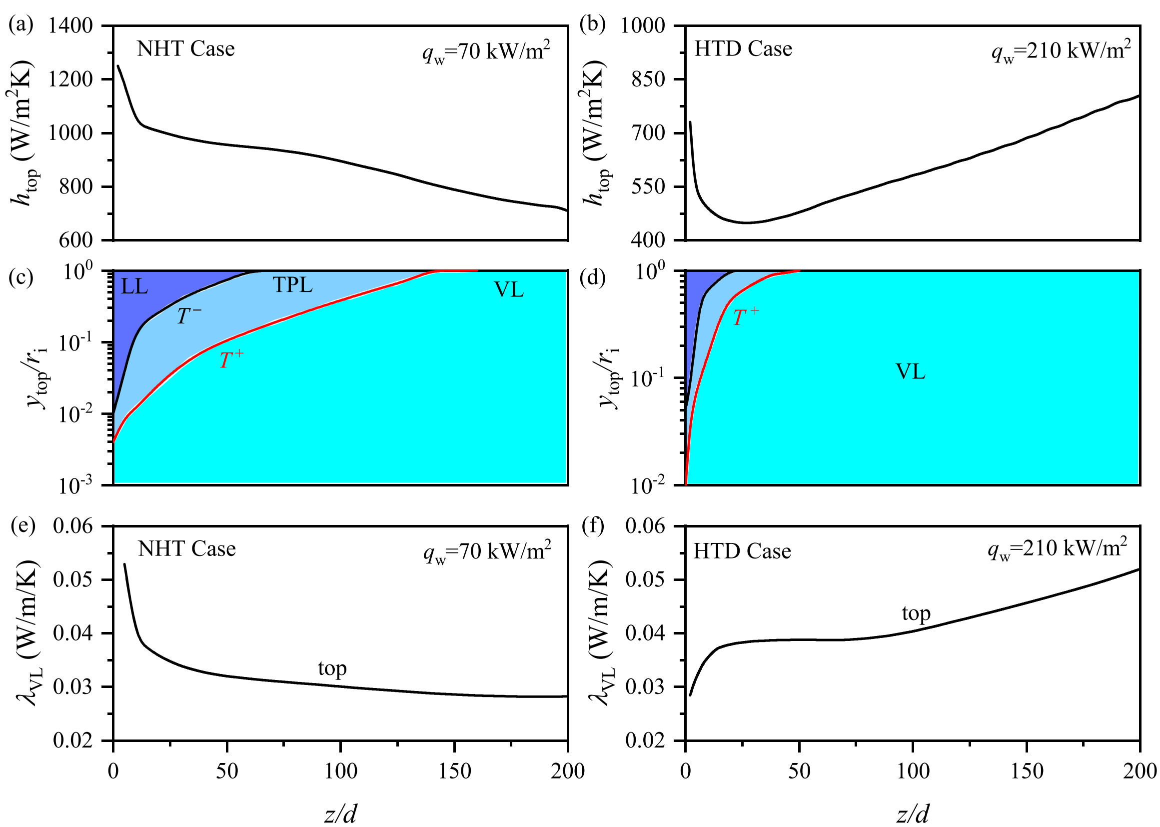

Fig. 7. Variations of heat transfer coefficient, phase distribution and physical properties along the flow direction at the top of the horizontal tube (P=8 MPa, G=300 kg/m^{2}s): (a), (c) and (e) are NHT case; (b), (d) and (f) are HTD case.

conductivity coefficient (see cyan region in Fig. 6). Fig. 6 shows that the thickness of VL film on tube top is larger than that on tube bottom ($\delta_{top}> \delta_{bot}$) for both NHT and HTD cases. Thus, $T_{wi,\ top}> T_{wi,\ bot}$ and $h_{bot}> h_{top}$ in Fig. 4 is confirmed. Compared with NHT, the HTD case behaves larger thickness of VL film, inducing higher wall temperature and lower heat transfer coefficient. Thus, Fig. 6 indicates that the VL film thickness is an important parameter in determining the supercritical heat transfer performance.

3.3. Phase distribution of sCO_2 along the flow direction

Fig. 6 only gives the phase distribution of supercritical fluid bulk in the horizontal tube at one cross-section. Figs. 7 and 8 compare the phase distribution along the flow direction with the variation tendency of heat transfer performance along the flow direction. It confirms that VL film thickness is the main parameter to determine the supercritical heat transfer performance. In addition, the effects of the thermal conductivity of the VL film and the heat capacity of the fluid bulk cannot be ignored in some regions and working conditions.

Fig. 7 shows the phase distribution of supercritical fluid bulk at the top of horizontal tube. It is found that the VL film thickness y_{top} increases along the flow direction until it reaches tube radius r_i. In the upstream region with y_{top}/r_i<1, the heat transfer coefficients h_{top} decrease along the flow direction for both NHT and HTD cases. It is attributed to the rising VL film thickness y_{top} along the flow direction (see Fig. 7a–d). However, in the downstream region with y_{top}/r_i=1, the variation tendency of h_{top} along the flow direction is reversed between the NHT case and HTD case. In such regions, thermal conductivity λ_{VL} instead of VL film thickness y_{top} controls the heat transfer performance. For supercritical fluid, there exists a critical temperature value T_c to distinguish different variation tendency of λ_{VL} versus T [57]. For example, such critical temperature is T_c=335.2 K at P=8 MPa. For NHT case, the fluid is heated to low temperature with $T_{pc}<T<T_c$, λ_{VL} decreases with rising T and z/d (see Fig. 7e). Thus, h_{top} still decreases along the flow direction in the downstream region (see Fig. 7a). However, for HTD case, the fluid is heated to high temperature with $T>T_c$, λ_{VL} increases with rising T and z/d (see Fig. 7f). As a result, h_{top} rises along the flow direction in the downstream region (see Fig. 7b).

Fig. 8 shows the phase distribution of supercritical fluid bulk at the bottom of the horizontal tube. For the NHT case, the thickness of VL film on the tube bottom y_{bot} keeps much smaller before z/d<100. In such regions, the effect of y_{bot} on heat transfer coefficient h_{bot} is weakened. Instead, the specific heat capacity c_p controls the variation tendency of h_{bot} along the flow direction, which was also reported in previous

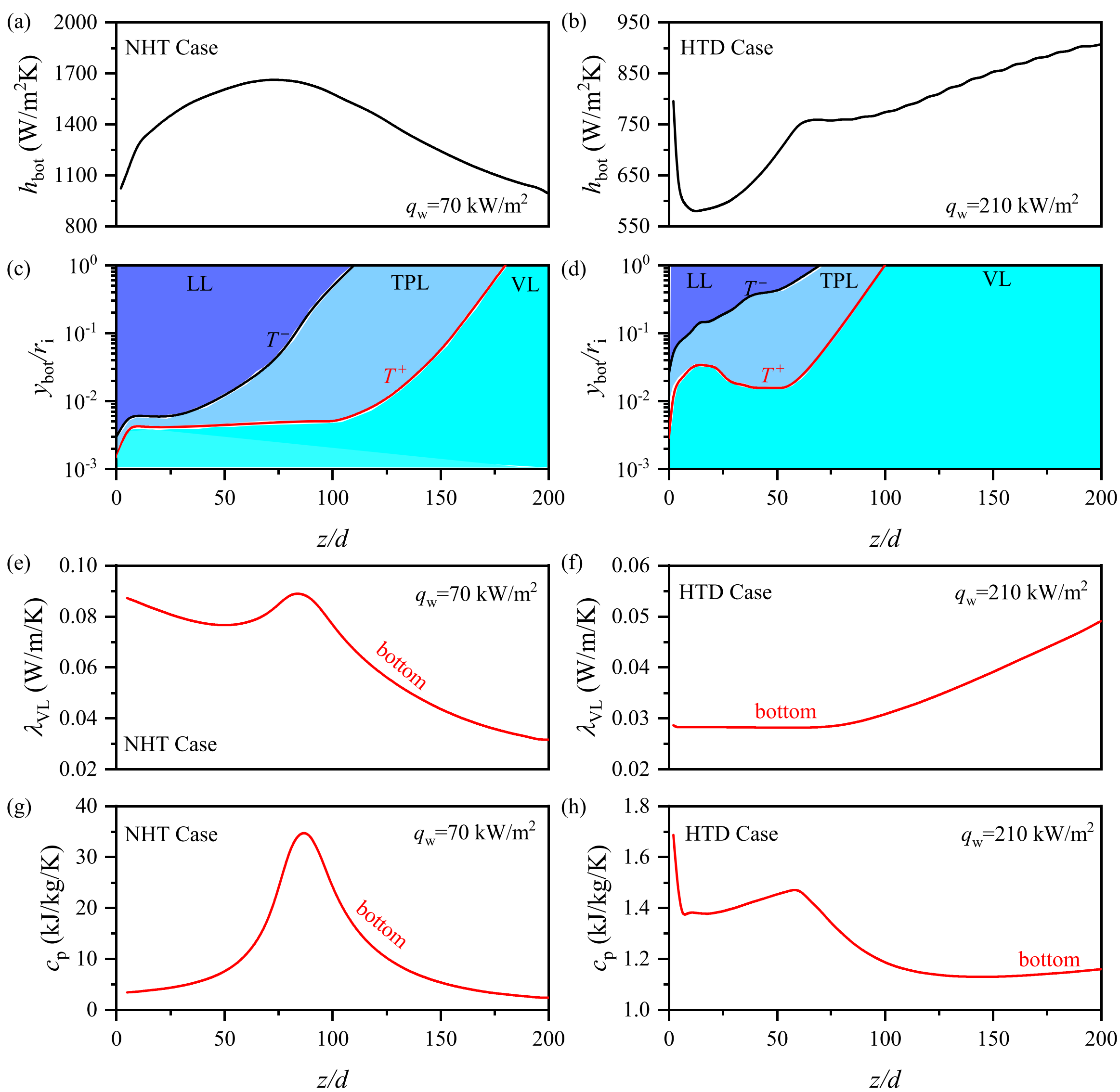

Fig. 8. Variations of heat transfer coefficient, phase distribution and physical properties along the flow direction at the bottom of the horizontal tube (P=8 MPa, G=300 kg/m^{2}s): (a), (c), (e) and (g)are NHT case; (b), (d), (f) and (h)are HTD case.

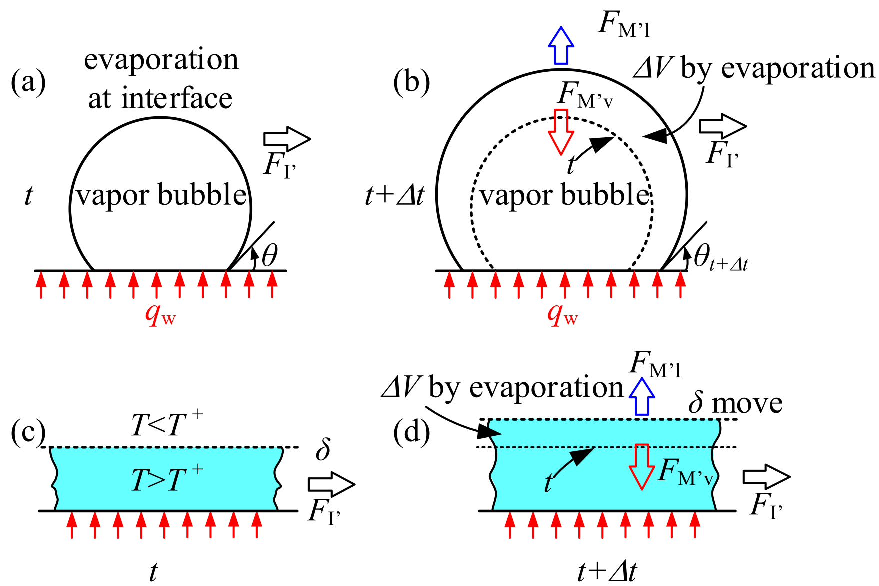

Fig. 9. K number reflects the competition between evaporation induced momentum force and inertia force. (a) and (b) for subcritical boiling; (c) and (d) for supercritical pseudo-boiling.

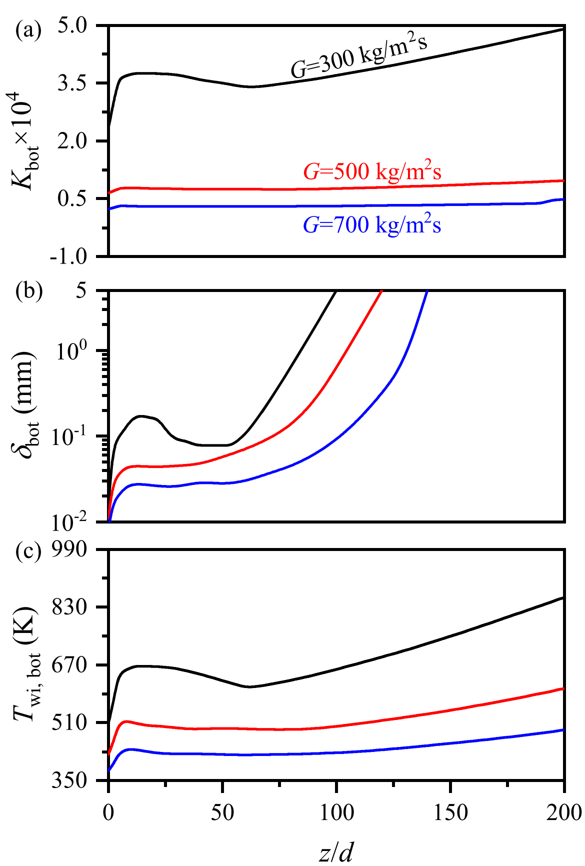

Fig. 10. Effect of different mass fluxes on heat transfer along the flow direction at the tube bottom (P=8 MPa, q_w=210 kW/m^2, θ=180°). (a) Variation of supercritical K_{bot} number with z/d; (b) Variation of vapor-like film thickness δ_{bot} with z/d; (c) Variation of inner wall temperature $T_{wi,\ bot}$ with z/d.

investigations [58,59]. Except for the above region with ultrathin VL film for the NHT case, the variation tendency of h_{bot} along the flow direction is determined by y_{bot} at upstream and λ_{VL} at downstream, respectively. The result and mechanism are similar to those shown in Fig. 7.

3.4. Supercritical K number to determine VL layer thickness

Figs. 6–8 indicates that VL film thickness is the main parameter to determine the supercritical heat transfer performance near the pseudo-critical condition. To explore the influence factors on VL film thickness, analogical analysis is performed between subcritical and supercritical heat transfer (See Fig. 9). For subcritical boiling, a vapor blanket generated on the heating wall from the coalescence of various bubbles can trigger the wall temperature overshoot and heat transfer deterioration HTD. To prevent HTD, vapor bubbles are desired to detach from the heating wall with small size. The bubble detachment size is determined by the competition between inertial force and evaporation momentum force. See Fig. 9a, the inertial force drives the bubble away from the wall, which is expressed as

$$F_{I'} = \frac{G^2 D}{\rho_l} \tag{15}$$

where G is the mass flux, D is the bubble diameter and ρ_l is the liquid density, respectively.

On the contrary, the evaporation momentum force is proposed by S. G. Kandlikar [60] to characterize the force to keep bubbles on the wall. During the boiling from t to $t+\Delta t$, the bubble volume expands ΔV with mass transfer from liquid to vapor, inducing compression of the surrounding liquid (see Fig. 9b). According to the action-reaction principle, the bubble is pressed on the wall by the evaporation momentum force, which is

$$F_{M'v} = \left(\frac{q_w}{i_{fg}}\right)^2 \frac{D}{\rho_v} \tag{16}$$

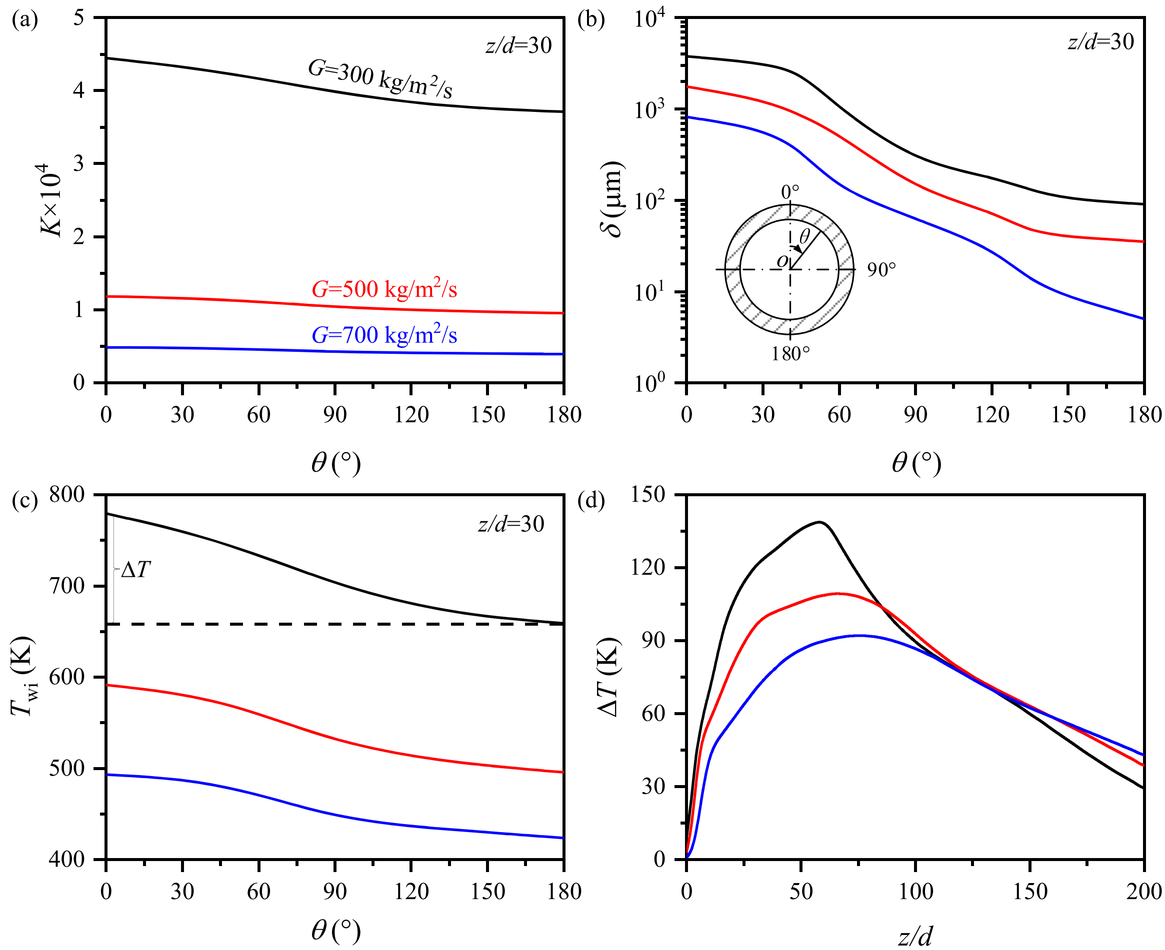

Fig. 11. Effect of different mass fluxes on circumferential heat transfer (P=8 MPa, q_w=210 kW/m^2): (a) Circumferential variation of supercritical K number; (b) Circumferential variation of vapor-like film thickness δ; (c) Circumferential variation of inner wall temperature T_{wi}; (d) Effect of different mass fluxes on ΔT.

where q_w is the heat flux, i_{fg} is the latent heat of evaporation, ρ_v is the density of vapor, respectively. To characterize the competition between evaporation momentum force and inertial force, the dimensionless K number is proposed, which is expressed as

$$K = \frac{F_{M'v}}{F_{I'}} = \left(\frac{q_w}{Gi_{fg}}\right)^2 \frac{\rho_l}{\rho_v} \tag{17}$$

A larger K number means evaporation momentum force overcomes inertial force to yield larger bubble detachment size, creating more risk of vapor blanket and HTD.

The previous investigations have proved that there is a lot of similarity between subcritical boiling and supercritical pseudo-boiling [25, 44]. Thus, Fig. 9c and Fig. 9d describe the inertial force and evaporation momentum force on the VL film, respectively. The supercritical K number is proposed to characterize the thickness of VL film δ, considering competition between evaporation momentum force and inertial force comprehensively. Based on analogical analysis, the supercritical K number may be

$$K = \left(\frac{q_w}{G\Delta i}\right)^2 \frac{\rho_{T^-}}{\rho_{T^+}} \tag{18}$$

where Δi is the pseudo-boiling enthalpy: [25]

$$\Delta i = \int_{T^-}^{T^+} c_p \mathrm{d}T = i(T^+) - i(T^-) \tag{19}$$

In Eq. (19), ρ_{T^-} and ρ_{T^+} are the liquid-like density at T^- and vapor-like density at T^+, respectively. The starting temperature T^- and ending temperature T^+ of supercritical pseudo-boiling defined in Fig. 5 is only determined by pressure. Thus, the supercritical K number defined in Eq. (19) remains almost constant for a case with set inlet pressure. It cannot characterize the change of VL film thickness along the flow direction and circumferential direction. In fact, different from the constant temperature in the vapor bubble for subcritical boiling, the temperature in supercritical VL film changes with T_w. Thus, the vapor-like density is better to be characterized with T_w. The supercritical K number is modified as follows:

$$K = \left(\frac{q_w}{G\Delta i}\right)^2 \frac{\rho_{T^-}}{\rho_{T_w}} \tag{20}$$

The supercritical K number in Eq. (20) can not only characterize the 3D changes of VL film thickness in the horizontal tube, but also reveal the HTD mechanism and influencing factors. For example, the supercritical K number increases with the rising heat flux q_w. As a result, the evaporation momentum force overcomes the inertial force to yield a

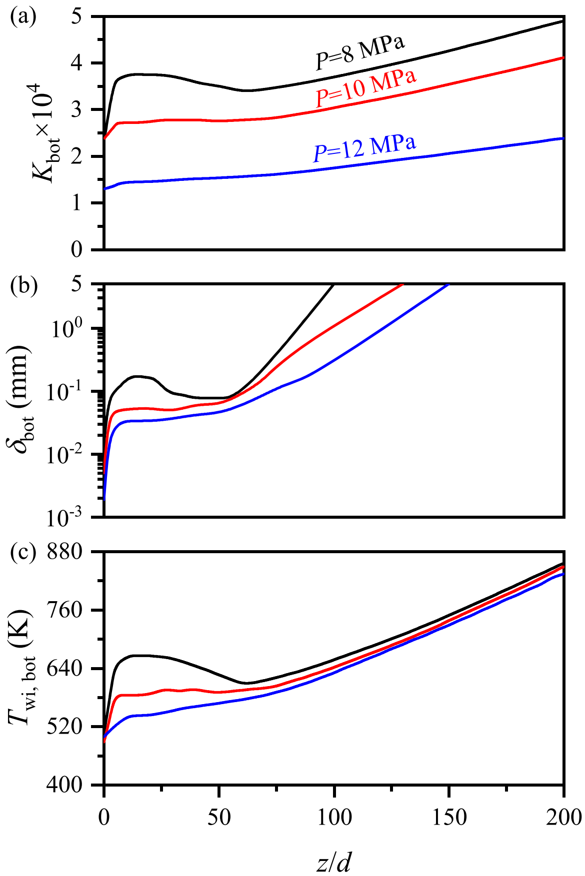

Fig. 12. Effect of different pressures on heat transfer along the flow direction at the tube bottom (G=300 kg/m^{2}s, q_w=210 kW/m^2, θ=180°). (a) Variation of supercritical K_{bot} number with z/d; (b) Variation of vapor-like film thickness δ_{bot} with z/d; (c) Variation of inner wall temperature $T_{wi,\ bot}$ with z/d.

thicker VL film. Thus, the HTD case occurs under high heat flux. It is logical and agrees well with the phase distribution in Fig. 6. More analysis of the supercritical K number on HTD mechanism is performed in the next section.

3.5. The effect of mass flux

HTD in horizontal tube induces not only wall temperature overshoot in the flow direction, but also serious wall temperature non-uniformity in the circumferential direction (see Fig. 4). It confirms that VL film thickness characterized by the supercritical K number is the key parameter to determine the supercritical heat transfer performance (see Figs. 6–8). Here, the influences of main operating condition parameters on HTD are analyzed based on the supercritical K number. Figs. 10–11 involve the effect of mass flux G and Figs. 12–13 involve the effect of pressure P, respectively.

According to Eq. (20), increasing mass flux G raises the inertia force to compete against evaporation momentum force, yielding smaller supercritical K number (see Fig. 10a). Correspondingly, the value of VL film thickness δ decreases and variation of δ with flow direction becomes smooth (see Fig. 10b). It means the supercritical heat transfer is enhanced. As a result, rising G decreases the wall temperature value T_{wi} and eliminates the wall temperature overshoot in flow direction (see Fig. 10c).

In addition, the effect of mass flux is similar between the flow direction and circumferential direction. In the circumferential direction, the variations trends of supercritical K, δ and T_{wi} are the same. See Fig. 11a–c, with increasing θ from top to bottom of horizontal tube, the wall temperature value T_{wi} decreases due to reducing supercritical K number and VL film thickness δ. What is more, the difference of supercritical K number between the top generatrix (θ=0°) and bottom generatrix (θ=180°) decrease with rising G. As a result, temperature difference ΔT between the top generatrix (θ=0°) and bottom generatrix (θ=180°) becomes smaller under lager G (see Fig. 11d). Thus, increasing mass flux is the effective method to repress the wall temperature overshoot and non-uniformity induced by HTD.

3.6. The effect of pressure

It is noted that the all results above are obtained under the pressure of 8 MPa, which is approaching the critical pressure. To improve system efficiency, heat exchangers may operate under higher pressure. Thus, it is necessary to discuss the effect of pressure on supercritical heat transfer performance. It is known that the pseudo-boiling enthalpy Δi increases with rising pressure P [61]. According to Eq. (20), the supercritical K number reduces with increasing pressure P (see Fig. 12a), yielding thinner VL film and lower wall temperature (see Fig. 12b–c). What is more, the temperature overshoot along the flow direction is also eliminated by raising the pressure (see Fig. 12c).

In the circumferential direction(see Fig. 13a–c), the higher pressure P always induces a smaller supercritical K number, thinner VL film and lower wall temperature from the top generatrix (θ=0°) to the bottom generatrix (θ=180°). However, both the supercritical K number and the temperature difference ΔT between the top generatrix (θ=0°) and bottom generatrix (θ=180°) change slightly with different pressure P from 8 MPa to 12 MPa (see Fig. 13d). Thus, increasing pressure only reduces wall temperature overshoot inducing by HTD but has a weak impact on wall temperature non-uniformity.

4. Conclusions

Heat transfer of sCO_2 in horizontal tube is investigated numerically. The pressure, mass flux and heat flux ranges are 8–12 MPa, 300–700 kg/m^{2}s, 70–210 kW/m^2, respectively. The mechanism and influence factors of heat transfer deterioration (HTD) are discussed based on pseudo-boiling theory. The main conclusions are summarized as follows.

- 3D phase distribution of supercritical fluid in a heated horizontal tube is obtained. Three regions are divided by the starting temperature $T^-$and ending temperature T^+ of supercritical pseudo-boiling, including the liquid-like (LL) core, transitional two phase-like (TPL) and vapor-like (VL) layer on the tube wall.
- It confirms that VL film thickness characterized by supercritical K number is the key parameter to determine the supercritical heat transfer performance near the pseudo-critical condition. Under high heat flux, a large supercritical K number with overwhelming evaporation momentum force to inertia force on VL film induces HTD.
- HTD in horizontal tube induces not only wall temperature overshoot in the flow direction, but also serious wall temperature non-uniformity in the circumferential direction. The maximal overshoot and circumferential difference of wall temperature reaches 114.2 °C and 138.7 °C, respectively.
- Increasing mass flux raises the inertia force to compete against the evaporation momentum force, yielding a smaller supercritical K number and thinner VL film. It is an effective method to repress both

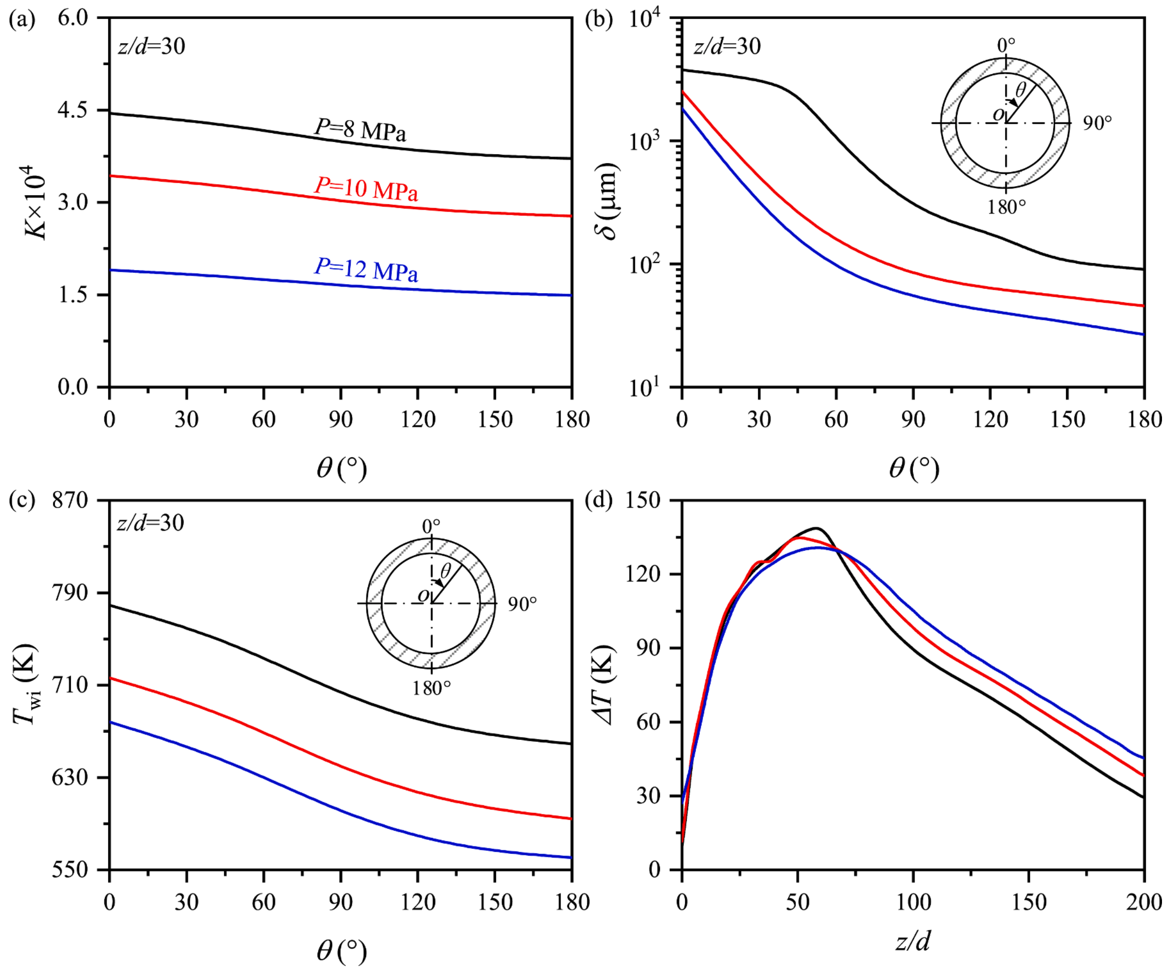

Fig. 13. Effect of different pressures on circumferential heat transfer (G=300 kg/m^{2}s, q_w=210 kW/m^2): (a) Circumferential variation of supercritical K number; (b) Circumferential variation of vapor-like film thickness δ; (c) Circumferential variation of inner wall temperature T_{wi}; (d) Effect of different pressures on ΔT.

the overshoot and non-uniformity of wall temperature induced by HTD.

- Rising pressure increases the pseudo-boiling enthalpy to reduce the supercritical K number and VL film thickness. It only reduces wall temperature value but has a weak impact on wall temperature non-uniformity.

CRediT authorship contribution statement

Bowen Yu: Writing – review & editing, Software, Methodology, Investigation, Formal analysis, Data curation. **Jian Xie:** Writing – original draft, Funding acquisition, Conceptualization. **Jinliang Xu:** Supervision, Resources, Project administration. **Liangyuan Cheng:** Visualization, Validation.

Declaration of competing interest

The authors declare that they have no known competing financial interests or personal relationships that could have appeared to influence the work reported in this paper.

Acknowledgments

The authors acknowledge the support from National Natural Science Foundation of China (No. 51821004 and No. 52130608).

Data availability

Data will be made available on request.

References

[1] F. Crespi, G. Gavagnin, D. Sánchez, G.S. Martínez, Supercritical carbon dioxide cycles for power generation: A review, Appl. Energy 195 (2017) 152–183.
[2] J. Yang, Z. Yang, Y. Duan, Design optimization and operating performance of S-CO2 brayton cycle under fluctuating ambient temperature and diverse power demand scenarios, J. Thermal Sci. 33 (1) (2023) 190–206.
[3] M.J. Li, H.H. Zhu, J.-Q. Guo, K. Wang, W.-Q. Tao, The development technology and applications of supercritical CO2 power cycle in nuclear energy, solar energy and other energy industries, Appl. Therm. Eng. 126 (2017) 255–275.
[4] Y.H. Fan, G.H. Tang, X.L. Li, D.L. Yang, General and unique issues at multiple scales for supercritical carbon dioxide power system: A review on recent advances, Energy Convers. Manage 268 (2022) 115993.
[5] K. Wang, Z.-D. Zhang, M.-J. Li, C.-H. Min, A coupled optical-thermal-fluid-mechanical analysis of parabolic trough solar receivers using supercritical CO2 as heat transfer fluid, Appl. Therm. Eng. 183 (2021) 116154.
[6] S. Zhang, X. Xu, C. Liu, X. Li, C. Wu, C. Dang, Experimental investigation and theoretical analysis on the heat transfer deterioration of supercritical CO2 in mixed and forced convection in vertical-straight tube with downward flow, Int. J. Heat. Mass Transf. 187 (2022) 122510.
[7] J. Xie, G. Xie, Assessment on heat transfer deterioration to supercritical carbon dioxide in upward flows via large eddy simulation, Int. J. Heat. Fluid. Flow. 95 (2022) 108954.
[8] S. Sahu, A.M. Vaidya, Evaluation of correlations for prediction of onset of heat transfer deterioration for vertically upward flow of supercritical water in pipe, Nuclear Eng. Technol. 53 (4) (2021) 1100–1108.
[9] D. Li, X. Xu, Y. Cao, C. Liu, S. Zhang, C. Dang, The characteristics and mechanisms of self-excited oscillation pulsating flow on heat transfer deterioration of supercritical CO2 heated in vertical upward tube, Appl. Therm. Eng. 202 (2022) 117839.

[10] Z. Yang, X. Luo, W. Chen, M.K. Chyu, Effects of longitudinal vortex generators on the heat transfer deterioration of supercritical CO2 in vertical tubes, Int. J. Heat. Mass Transf. 152 (2020) 119478.
[11] J. Xie, D. Liu, H. Yan, G. Xie, S.K.S. Boetcher, A review of heat transfer deterioration of supercritical carbon dioxide flowing in vertical tubes: heat transfer behaviors, identification methods, critical heat fluxes, and heat transfer correlations, Int. J. Heat. Mass Transf. 149 (2020) 119233.
[12] J.D. Jackson, Fluid flow and convective heat transfer to fluids at supercritical pressure, Nuclear Eng. Des. 264 (2013) 24–40.
[13] S. Liu, Y. Huang, G. Liu, J. Wang, L.K.H. Leung, Improvement of buoyancy and acceleration parameters for forced and mixed convective heat transfer to supercritical fluids flowing in vertical tubes, Int. J. Heat. Mass Transf. 106 (2017) 1144–1156.
[14] Y.-L. Cui, H.-X. Wang, Experimental study on convection heat transfer of R134a at supercritical pressures in a vertical tube for upward and downward flows, Appl. Therm. Eng. 129 (2018) 1414–1425.
[15] D.E. Kim, M.H. Kim, Experimental study of the effects of flow acceleration and buoyancy on heat transfer in a supercritical fluid flow in a circular tube, Nuclear Eng. Des. 240 (10) (2010) 3336–3349.
[16] J.D. Jackson, Models of heat transfer to fluids at supercritical pressure with influences of buoyancy and acceleration, Appl. Therm. Eng. 124 (2017) 1481–1491.
[17] B. Zhu, J. Xu, H. Zhang, J. Xie, M. Li, Effect of non-uniform heating on scCO2 heat transfer deterioration, Appl. Therm. Eng. 181 (2020) 115967.
[18] D. Huang, W. Li, A brief review on the buoyancy criteria for supercritical fluids, Appl. Therm. Eng. 131 (2018) 977–987.
[19] D. Huang, Z. Wu, B. Sunden, W. Li, A brief review on convection heat transfer of fluids at supercritical pressures in tubes and the recent progress, Appl. Energy 162 (2016) 494–505.
[20] J. Xu, Y. Wang, X. Ma, Phase distribution including a bubble like region in supercritical fluid, Phys. Rev. E 104 (1) (2021) 014142.
[21] G.G. Simeoni, T. Bryk, F.A. Gorelli, M. Krisch, G. Ruocco, M. Santoro, T. Scopigno, The Widom line as the crossover between liquid-like and gas-like behaviour in supercritical fluids, Nat. Phys. 6 (7) (2010) 503–507.
[22] X. He, J. Xu, X. Yu, J. Xie, Distinguishing evaporation-like and boiling-like modes of pseudo-boiling in supercritical pressures, Int. J. Heat. Mass Transf. 214 (2023) 124417.
[23] F. Maxim, C. Contescu, P. Boillat, B. Niceno, K. Karalis, A. Testino, C. Ludwig, Visualization of supercritical water pseudo-boiling at Widom line crossover, Nat. Commun. 10 (2019) 4114.
[24] D.T. Banuti, Crossing the Widom-line – Supercritical pseudo-boiling, J. Supercrit. Fluids. 98 (2015) 12–16.
[25] Q. Wang, X. Ma, J. Xu, M. Li, Y. Wang, The three-regime-model for pseudo-boiling in supercritical pressure, Int. J. Heat. Mass Transf. 181 (2021) 121875.
[26] N.L. Kafengauz, M.I. Fedorov, Excitation of high-frequency pressure oscillations during heat exchange with diisopropylcyclohexane, J. Eng Phys. 11 (1) (1966) 63–67.
[27] J.W. Ackerman, Pseudo-boiling heat transfer to supercritical pressure water in smooth and ribbed tubes, J. Heat Transf. 92 (1970) 490.
[28] B. Zhu, J. Xu, X. Wu, J. Xie, M. Li, Supercritical "boiling" number, a new parameter to distinguish two regimes of carbon dioxide heat transfer in tubes, Int. J. Thermal Sci. 136 (2019) 254–266.
[29] J. Xu, H. Zhang, B. Zhu, J. Xie, Critical supercritical-boiling-number to determine the onset of heat transfer deterioration for supercritical fluids, Solar Energy 195 (2020) 27–36.
[30] C. Yan, J. Xu, S. Wang, G. Liu, Numerical study of convective heat transfer to supercritical CO2 in vertical heated tubes, Int. Commun. Heat Mass Transf. 137 (2022) 106242.
[31] X.L. Li, X.Y. Yu, P.T. Liu, Y.H. Fan, D.L. Yang, G.H. Tang, S-CO2 flow in vertical tubes of large-diameter: experimental evaluation and numerical exploration for heat transfer deterioration and prevention, Int. J. Heat. Mass Transf. 216 (2023) 124563.
[32] N. Longmire, D.T. Banuti, Onset of heat transfer deterioration caused by pseudo-boiling in CO2 laminar boundary layers, Int. J. Heat. Mass Transf. 193 (2022) 122957.
[33] Q. Li, Z.J. Lin, L. Yang, Y. Wang, Y. Li, W.H. Cai, Micro segment analysis of supercritical methane thermal-hydraulic performance and pseudo-boiling in a PCHE straight channel, Pet. Sci. 21 (2) (2024) 1275–1289.
[34] Z. Yang, H. Wang, B. Guan, H. Yang, Z. Li, G. Wang, Experimental and numerical investigation on the mechanisms of novel heat transfer deterioration of supercritical CO2 in vertical tubes, Int. Commun. Heat Mass Transf. 153 (2024) 107384.
[35] Y. Ai, H. Wu, T. Lee, C. Lee, X. Li, Theoretical analysis of the three-stage phase transition process of alkane droplet under supercritical conditions, Int. J. Heat. Mass Transf. 225 (2024) 125381.
[36] B. Yuan, W. Wang, G. Xin, W. Du, Numerical analysis of heat transfer characteristics to supercritical CO2 in a vertical mini-channel: transition and pseudo-boiling, J. Thermal Sci. 33 (1) (2023) 101–113.
[37] W. Dong, W. Wei, L. Zhao, L. Zhang, T. Zhou, J. Ba, The impact of the pseudo-boiling on the thermal behaviors of supercritical CO2, Numer. Heat Transf. Part A: Appl. 84 (3) (2022) 238–251.
[38] M. Pizzarelli, The status of the research on the heat transfer deterioration in supercritical fluids: A review, Int. Commun. Heat Mass Transf. 95 (2018) 132–138.
[39] Y. Jin, Z. Li, N. Yuan, Y. Yao, Y. Zhai, Z. Li, Flow and heat transfer of supercritical water in a rifled tube with axially non-uniform heating, Appl. Therm. Eng. 169 (2020) 114923.
[40]] G.A. Adebiyi, W.B. Hall, Experimental investigation of heat transfer to supercritical pressure carbon dioxide in a horizontal pipe, Int. J. Heat. Mass Transf. 19 (7) (1976) 715–720.
[41] S.R. Pidaparti, J.A. McFarland, M.M. Mikhaeil, M.H. Anderson, D. Ranjan, Investigation of buoyancy effects on heat transfer characteristics of supercritical carbon dioxide in heating mode, J. Nucl. Eng. Radiat. Sci. 1 (3) (2015) 031001.
[42] T.H. Kim, J.G. Kwon, M.H. Kim, H.S. Park, Experimental investigation on validity of buoyancy parameters to heat transfer of CO2 at supercritical pressures in a horizontal tube, Exp. Therm. Fluid. Sci. 92 (2018) 222–230.
[43] S.M. Liao, T.S. Zhao, An experimental investigation of convection heat transfer to supercritical carbon dioxide in miniature tubes, Int. J. Heat. Mass Transf. 45 (2002) 5025–5034.
[44] C. Zhang, B. Hao, L. Cheng, J. Xu, Q. Wang, Heat transfer characteristics of CO2 in a horizontal tube under subcritical and supercritical pressures, Heat Transf. Eng. 45 (4-5) (2023) 399–416.
[45] L. Cheng, Q. Wang, J. Xu, Supercritical heat transfer of CO2 in horizontal tube emphasizing pseudo-boiling and stratification effects, Int. J. Heat. Mass Transf. 220 (2024) 124953.
[46] L. Cheng, J. Xu, Q. Wang, X. Dong, The influence of tube diameter parameters on the flow resistance and heat transfer characteristics of supercritical CO2 in horizontal tubes, Appl. Therm. Eng. 241 (2024) 122361.
[47] L. Cheng, J. Xu, W. Cao, K. Zhou, G. Liu, Supercritical carbon dioxide heat transfer in horizontal tube based on the Froude number analysis, Energy 294 (2024) 130980.
[48] Z. Li, Y. Wu, G. Tang, D. Zhang, J. Lu, Comparison between heat transfer to supercritical water in a smooth tube and in an internally ribbed tube, Int. J. Heat. Mass Transf. 84 (2015) 529–541.
[49] C. Yan, J. Xu, B. Zhu, G. Liu, Numerical analysis on heat transfer characteristics of supercritical CO2 in heated vertical up-flow tube, Materials 13 (3) (2020) 723.
[50] X.L. Li, G.X. Li, G.H. Tang, Y.H. Fan, D.L. Yang, A generalized thermal deviation factor to evaluate the comprehensive stress of tubes under non-uniform heating, Energy 263 (2023) 125710.
[51] Y. Li, F. Sun, G. Xie, B. Sunden, J. Qin, Numerical investigation on flow and thermal performance of supercritical CO2 in horizontal cylindrically concaved tubes, Appl. Therm. Eng. 153 (2019) 655–668.
[52] K. Wang, X. Xu, Y. Wu, C. Liu, C. Dang, Numerical investigation on heat transfer of supercritical CO2 in heated helically coiled tubes, J. Supercrit. Fluids. 99 (2015) 112–120.
[53] J. Wang, J. Yang, J. Gong, C. Zhao, K. Hooman, A designed wall roughness approach to improve turbulent heat transfer to supercritical CO2 flowing in horizontal tubes, J. Supercrit. Fluids. 190 (2022) 1105738.
[54] F.R. Menter, Two-equation eddy-viscosity turbulence models for engineering applications, AIAA J. 32 (8) (1994) 1598–1605.
[55] ANSYS Fluent 15.0, Solver Theory Guide, ANSYS Inc, 2013.
[56] E.W. Lemmon, M.L. Huber, M.O. Mclinden, NIST Standard Reference Database 23: Reference Fluid Thermodynamic and Transport properties-REFPROP, 9.0, NIST NSRDS, 2010.
[57] B. Yu, X. He, J. Xu, Experiment and numerical simulation of supercritical CO2 pool heat transfer (in Chinese), Sci. Sin. Technol. 54 (2024) 636–644, https://doi.org/10.1360/SST-2022-0325.
[58] S. Mao, T. Zhou, D. Wei, H. Lu, W. Liu, Numerical modeling on heat transfer of supercritical water in cooled horizontal circular tube, J. Supercrit. Fluids. 191 (2022) 105769.
[59] X. Huang, Q. Wang, Z. Song, Y. Yin, H. Wang, Heat transfer characteristics of supercritical water in horizontal double-pipe, Appl. Therm. Eng. 173 (2020) 115191.
[60] S.G. Kandlikar, Heat transfer mechanisms during flow boiling in microchannels, J. Heat. Transfer. 126 (2014) 8–16.
[61] B. Zhu, J. Xu, C. Yan, J. Xie, The general supercritical heat transfer correlation for vertical up-flow tubes: K number correlation, Int. J. Heat. Mass Transf. 148 (2020) 119080.